Influence of CdS films synthesized by different methods on the photovoltaic performance of CdTe/CdS thin film solar cells*

Jun Wang(汪俊)[1,†], Yuquan Wang(王玉全)[1], Cong Liu(刘聪)[1], Meiling Sun(孙美玲)[1], Cao Wang(王操)[1], Guangchao Yin(尹广超)[1], Fuchao Jia(贾福超)[1], Yannan Mu(牟艳男)[2], Xiaolin Liu(刘笑林)[1], and Haibin Yang(杨海滨)[3,‡]

[1] *School of Physics and Optoelectronic Engineering, Shandong University of Technology, Zibo* 255000, *China*
[2] *Department of Physics and Chemistry, Heihe University, Heihe* 164300, *China*
[3] *State Key Laboratory of Superhard Materials, Jilin University, Changchun* 130012, *China*

(Received 12 March 2020; revised manuscript received 30 June 2020; accepted manuscript online 7 August 2020)

The cadmium sulphide (CdS) film is grown on cadmium telluride (CdTe) nanorods (NRs) arrays by different methods such as chemical bath deposition (CBD), magnetron sputtering (MS), and homogenous precipitation (HP) techniques. The impact of various deposition methods is explored in detail on the growth of CdTe/CdS composite film, the CdTe/CdS interface property, and solar cell efficiency. Compared to the CBD and HP methods, the MS method can improve the growth of the CdS on CdTe NRs with high crystalline quality. The device based on the CdS film prepared by the MS method demonstrates excellent photovoltaic performance, which has the potential for applications in solar cells.

Keywords: CdS, chemical bath deposition, magnetron sputtering, homogenous precipitation

PACS: 88.30.mj, 88.40.H−, 88.40.jm **DOI:** 10.1088/1674-1056/abad22

1. Introduction

CdS films appear as the most popular materials in the large-scale manufacturing of thin-film solar cells because of their direct optical band gap of 2.42 eV and high optical transmittance, especially in CdTe based photovoltaic devices.[1–3] Various methods have been employed for the preparation of CdS thin films such as the chemical bath deposition (CBD), thermal evaporation, electrodeposition, magnetron sputtering (MS), and homogenous precipitation (HP).[4–9] Among these growth techniques, the CBD is a simple and low-cost method for the fabrication of CdS films, and numerous investigations have been undertaken to obtain CdS films by this method. The CBD is generally carried out in an aqueous alkaline solution to release Cd^{2+} and S^{2-} ions and ammonium hydroxide is commonly used as the complexing agent.[10,11] As for the HP method, the gradual and even thermal decomposition of urea can result in a highly uniform increase in the pH of the solution, which can control the particle size and uniformity of the CdS film.[12–15] In addition, the MS method is also a proven well productive method for the CdTe solar cells.[16,17] In the field of materials science, it is well-known that the deposition techniques and growth conditions have an important influence on the quality and characteristic of the growing layer. Therefore, many research advances focus on the effect of the deposition method on the properties of CdS films. Remarkable differences in the properties of CdS films deposited by different methods have been studied in detail.[18–20] In addition, in the case of the CdTe solar cell, as the energy converting interface, the interface property of CdS/CdTe can also vary depending on the layer growth technique. Nevertheless, to the best of our knowledge, the impact of the CdS layer on the interfacial property is rarely investigated. Therefore, a more refined understanding of the CdS/CdTe interface is necessary.[21–24]

In this paper, the electrochemical deposition method is employed to prepare high density vertically CdTe NRs arrays on the Ni substrate. Different methods such as the CBD, HP, and MS are then served for the preparation of the CdS on CdTe NRs. The differences in the properties of the CBD, HP, and MS synthesized CdS films on CdTe NRs arrays are investigated in detail. The impact of CdS films fabricated by different methods on the interfacial property of CdTe/CdS and solar cell efficiency is also studied. Based on the results, the CdTe/MS-CdS solar cell has a better photovoltaic behavior due to the better coverage and crystalline of the CdS film on CdTe NRs arrays.

2. Experiments

2.1. Fabrication of the CdTe/CdS thin film

The TiO_2 Electrodeposition method is utilized for the preparation of CdTe nanorods (NRs) arrays.[25,26] The electrodeposition process is carried out in a three-electrode electrochemical cell. The Ni foil, graphite plate, and saturated silver/silver chloride (Ag|AgCl|KCl(sat)) are used as the working electrode, counter electrode, and reference electrode, re-

*Project supported by Natural Science Foundation of Shandong Province, China (Grant No. ZR2019QF018), National Natural Science Foundation of China (Grant Nos. 61904098 and 11904209), and Natural Science Foundation of Heilongjiang Province of China (Grant No. 2017001).

†Corresponding author. E-mail: junwang1819@163.com
‡Corresponding author. E-mail: yanghb@jlu.edu.cn

spectively. CdTe NRs are synthesized at −0.5 V for 60 min. After each deposition, the as-synthesized CdTe films are thoroughly washed with distilled water, and then dried in air. Finally, in order to improve the crystal quality, the films are annealed at 300 °C for 30 min in a flowing N_2 atmosphere, and used for deposition of the CdS film. The schematic of a three-electrode electrochemical cell and FESEM image of the CdTe NRs array film are shown in Fig. S1. In this work, CdS films are deposited on the CdTe layer using three different methods.

2.1.1. Fabrication of the CdS by the CBD method

The CdS is grown on CdTe NRs arrays by the CBD technique according to previous reports.[27] Briefly, CdTe films are firstly placed vertically inside the beaker and immersed into the chemical bath solution containing 0.02 M $CdCl_2{\cdot}2.5H_2O$, 0.5 M KOH, 1.5 M NH_4NO_3, and 0.2 M CH_4N_2S. Then the deposition is performed at a bath temperature of 80 °C for 40 min. In order to obtain a compact CdS layer on CdTe NRs arrays, multiple depositions are employed. After each deposition, the CdTe/CdS composite film is washed ultrasonically to remove impurities from the surface and minimize the loosely adhered CdS particles on CdTe NRs, and finally dried in air for further experimental tests.

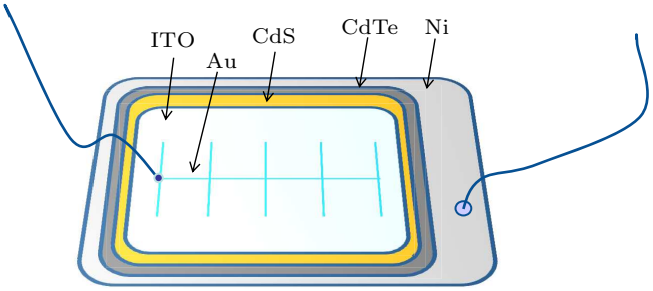

Scheme 1. Schematic diagram of the Ni/CdTe/CdS/ITO/Au thin film solar cell.

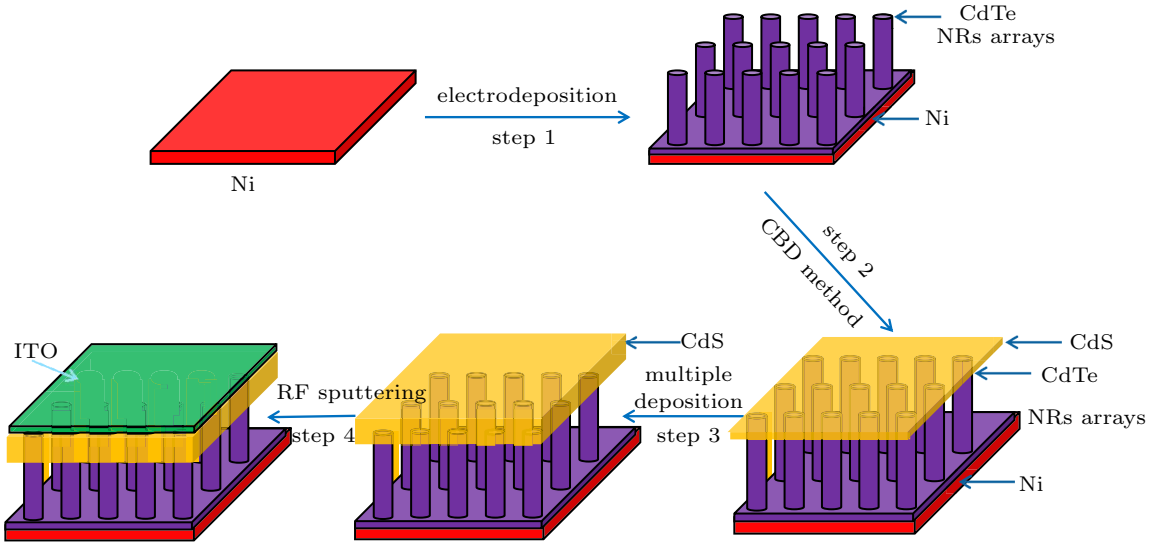

Scheme 2. Schematic illustration describing the overall process of device fabrication based on CBD-CdS film.

2.1.2. Fabrication of the CdS by the HP method

As for the HP method, in comparison with the CBD method, the reagents used for the bath solution are thiourea, cadmium chloride, urea, and deionized water. Due to the gradual and even thermal decomposition of urea, better control of synthesis for CdS thin films can be achieved. The concentration values and the bath temperature could be found in our previous paper.[9]

2.1.3. Fabrication of the CdS by the MS method

A homemade thin film magnetron sputtering deposition system is used to deposit CdS films. Prior to sputtering, to remove contaminations on the target surface, the CdS target is pre-sputtered for 15 min. To reduce the damage to the surface of CdTe film during the sputtering process, the films are deposited under Ar:O_2 (ratio: 1.5%) atmosphere with a pressure of 30 mTorr. The deposition is carried out for 20 min with a power of 50 W. The substrate temperature is kept at room temperature.

2.2. Photovoltaic device fabrication

Before device fabrication, the as-deposited CdS films on CdTe NRs arrays by the CBD, HP, MS methods are referred to as the CdTe/CBD-CdS, CdTe/HP-CdS, and CdTe/MS-CdS, respectively. All the deposited films are coated with a saturated $CdCl_2$-methanol solution and then annealed in N_2 atmosphere at 400 °C for 30 min to achieve suitable recrystallization for practical use. After cooling to room temperature, indium tin oxide (ITO) layer is deposited subsequently by the MS method for 15 min with a power of 50 W. Finally, the device with substrate configuration of Ni/CdTe NRs arrays/CdS/ITO/Au is completed by depositing an Au electrode on the surface of the ITO through sputtering (Scheme 1). The overall fabrication for the CdTe/CBD-CdS, CdTe/HP-CdS, and CdTe/MS-CdS solar

cells are exhibited in Schemes 2–4.

2.3. Characterization

The structural properties of the deposited films are determined using an x-ray diffractometer (XRD, Rigaku D/max-2500, with Cu $K\alpha$ radiation, $\lambda = 1.5418$ Å). The scanning range is between 20° and 80°. Field-emission scanning electron microscopy (FESEM) imaging is performed on a JSM-6700F JEOL microscope to investigate the surface morphologies of the films. Current density–voltage (J–V) curves are measured by using a solar simulator under AM 1.5G light illumination to obtain photoelectric properties. All the measurements are performed at room temperature.

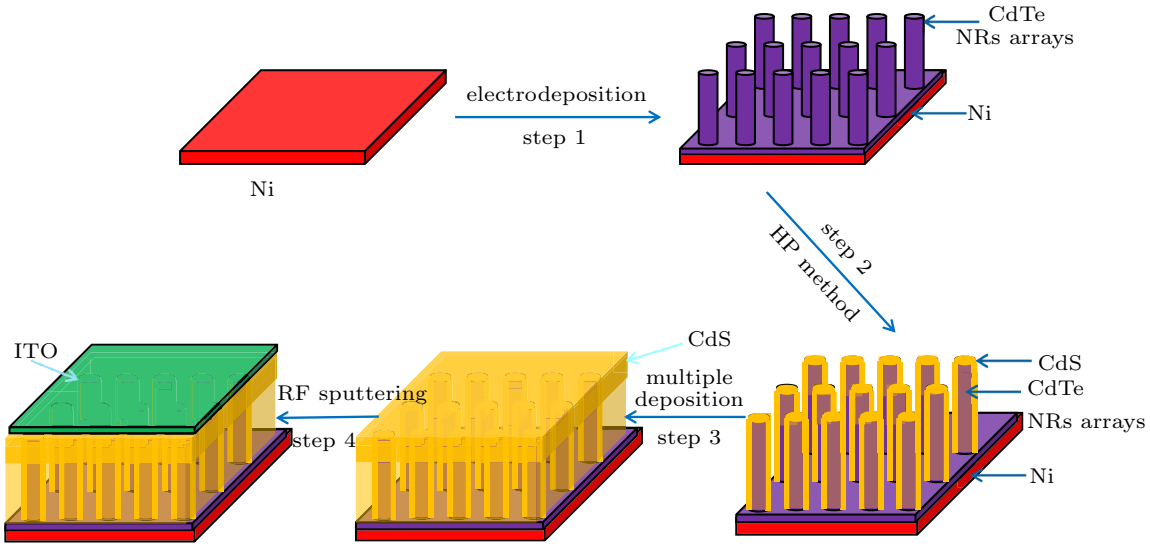

Scheme 3. Schematic illustration describing the overall process of device fabrication based on the HP-CdS film.

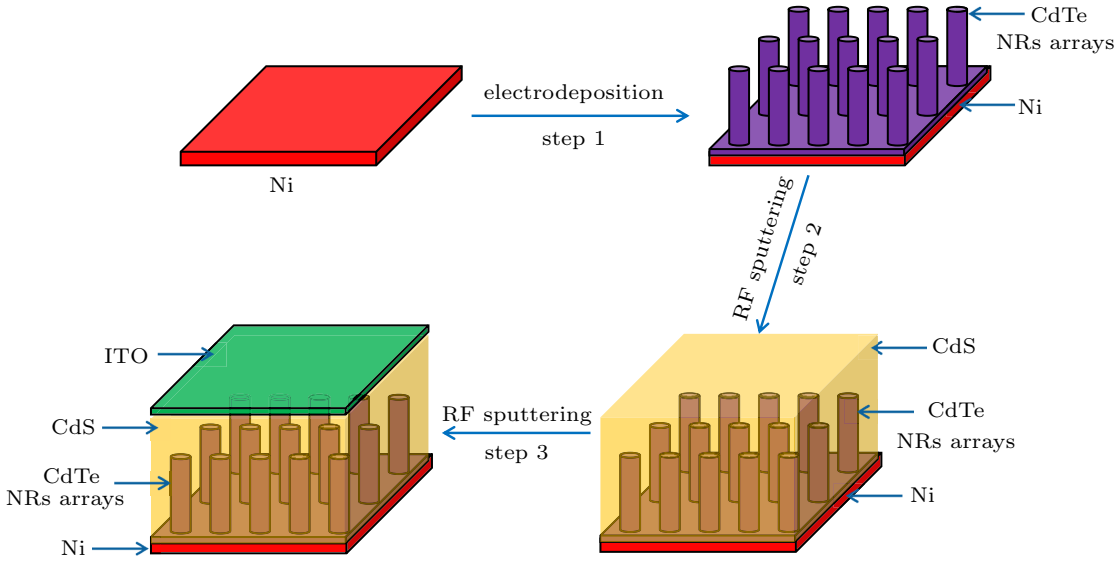

Scheme 4. Schematic illustration describing the overall process of device fabrication based on the MS-CdS film.

3. Results and discussion

The typical XRD patterns of the synthesized CdTe/CBD-CdS, CdTe/HP-CdS, and CdTe/MS-CdS films are illustrated in Fig. 1. By analyzing the patterns, apart from the Ni and Ni_2Te_3 diffraction peaks, the characteristic diffraction peaks at $2\theta = 23.98°$, 39.70°, and 49.90° which corresponds to (111), (220), and (311) planes, respectively, are assigned to the cubic phase of CdTe. The diffraction peaks at 2θ of 24.91°, 26.63°, 28.29°, 36.73°, 43.78°, and 47.93° demonstrate crystalline planes (100), (002), (101), (102), (110), and (103) of hexagonal phase CdS, indicating the successful deposition of the CdS on CdTe NRs by the CBD, HP, and MS methods. Peaks from the oxides of CdO and TeO_x are not observed. Noticeably, a clear variation of the diffracted peak intensity can be observed in Fig. 1. The CBD method is creates the CdS with poor crystalline quality that can be ascribed to the higher

reaction speed in the CBD approach compared with the HP method. The sharp and strong peaks of CdS made by the MS method confirm that the product is well crystallized with high purity. The improvement of film quality is favorable to charge transport.

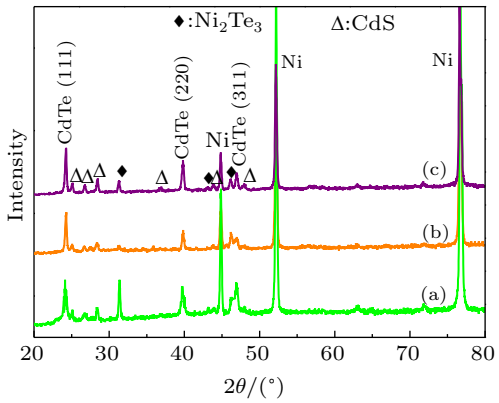

Fig. 1. XRD patterns of the (a) CdTe/CBD-CdS film, (b) CdTe/HP-CdS film, and (d) CdTe/MS-CdS film.

Figures 2–4 exhibit the FESEM images of the CdTe/CdS composite films prepared by various methods, which clearly display the different growth conditions of the CdS on CdTe NRs array films. The growth of CdS films is highly dependent on the deposition methods as perceptible from the FESEM images. In Fig. 2(a), it can be observed that a thin CdS layer can be formed on the top of CdTe NRs arrays because of the rapid deposition of the CdS film in the alkaline solution. Inset of Fig. 2(a) shows that the CdS layer is comprised of a number of cracks. Some voids between the thin CdS layer and CdTe NRs can also be observed. With increasing the cycles of CdS deposition (Fig. 2(b)), the surface of the CdS layer becomes smooth. However, the voids between CdS and CdTe NRs can also be distinctly observed. These voids can cause a poor quality p–n junction, which results in charge recombination. Furthermore, it is found, in experiments, the adhesion between the CdTe and Ni substrate becomes poor, which can be attributed to the alkaline environment in the deposition process.

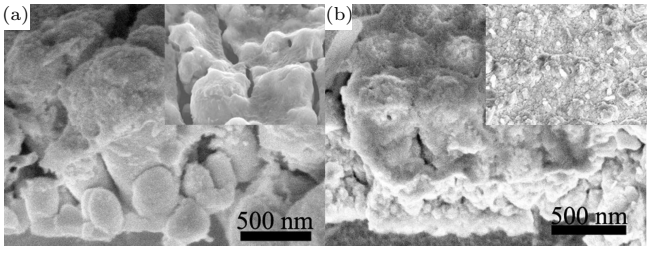

Fig. 2. FESEM images of CdTe/CBD-CdS films with different deposition cycles: (a) 1 cycle and (b) 3 cycles.

FESEM images of the CdTe/HP-CdS films are given in Fig. 3. As shown in Fig. 3(a), it is interesting to note that CdS nanoparticles enter into the CdTe NRs arrays slowly and embrace the NRs tightly. After multiple depositions, the CdS occupies nearly the entire space surrounding the CdTe NRs, and a compact CdS layer (∼ 200 nm) without any cracks and pinholes can be formed on the top of CdTe NRs (the inset of Fig. 3(b)). Besides, remarkably, the CdTe still maintains the rod-like pattern well, suggesting that the deposition of the CdS by the HP method has no significant negative influence on CdTe nanostructures.

The cross-sectional and top-view FESEM images of the CdTe/CdS film deposited by the MS method are shown in Fig. 4. It can be observed that each CdTe NRs is wrapped with the CdS and a uniform CdS layer is grown on the top surface of the CdTe NRs. In comparison to the CdS film synthesized by the HP method, the CdS particles become larger and the grain boundaries reduce significantly.

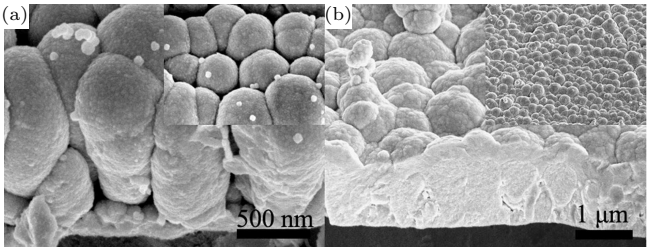

Fig. 3. FESEM images of CdTe/HP-CdS films with different deposition cycles: (a) 1 cycle and (b) 3 cycles.

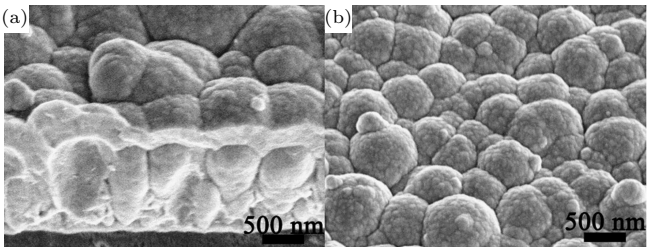

Fig. 4. The cross-section (a) and the top surface (b) FESEM images of CdTe/MS-CdS films.

According to the discussion above, it can be seen that the morphology of the CdTe/CdS composite film is greatly dependent on its deposition methods. In comparison to the CBD method, a better coverage of CdS film onto CdTe NRs can be achieved by the HP method. This phenomenon can be explained as follows. As for the HP method, due to the gradual and even thermal decomposition of urea, the pH of the solution can change slowly to prevent the rapid precipitation of CdS nanoparticles. Finally, the CdS film with controlled particle size and uniformity can be deposited on the CdTe NRs arrays successfully. In contrast, the CBD method is usually carried out in an ammoniacal alkaline solution,[28] which can lead to a rapid change of solution concentration. The reagents do not have enough time for the nucleation process, resulting in inefficient coverage of the CdS on the CdTe NRs arrays. Furthermore, as illustrated previously in Figs. 3 and 4, the as-prepared CdTe/CdS film shows no obvious differences between HP and MS methods. After careful analysis, it can be found that the

crystalline size of the CdS film deposited by the MS method is bigger than that of the CdS film deposited by the HP method. This can be attributed to the distant migration of the sputtered atoms, thus forming a dense film with larger grains and lower defects by the MS method.

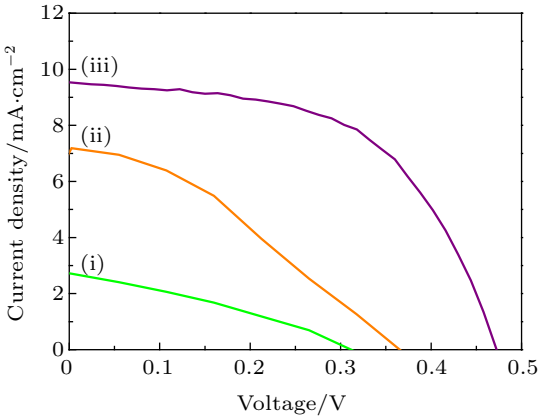

Fig. 5. The J–V curves of (i) CdTe/CBD-CdS solar cell, (ii) CdTe/HP-CdS solar cell, and (iii) CdTe/MS-CdS solar cell.

The performance of different CdTe/CdS solar cells prepared using different methods is presented in Fig. 5. The detailed device parameters are listed in Table 1. For the CdTe/CBD-CdS solar cell, the values of V_{oc}, J_{sc}, and FF are 0.32 V, 2.71 mA/cm^2, and 0.31, respectively, and the efficiency is limited by low J_{sc}. The low J_{sc} values indicate serious carrier recombination at the CdTe/CdS heterojunction, in combination with the FESEM results depicted in Fig. 2. With the HP-CdS film as a window layer, the device generates V_{oc}, J_{sc}, and FF of 0.37 V, 7.00 mA/cm^2, and 0.34, corresponding to a photoelectric conversion efficiency of 0.88 (Table 1). All of the device parameters are considerably enhanced in comparison with those of the device based on the CBD-CdS (Fig. 4). This can be ascribed to the larger heterojunction area of the CdTe/HP-CdS solar cell, in contrast to the CdTe/CBD-CdS solar cell, which can ensure efficient separation of photogenerated carriers. Solar cell with maximum efficiency is obtained by using the MS-CdS film as a window layer. The maximum efficiency obtained in our study is 2.50% (Fig. 4), exhibiting J_{sc} of 9.51 mA/cm^2, V_{oc} of 0.47 V, and FF of 0.56. The simultaneous improvement of V_{oc}, J_{sc}, and FF is strongly associated with the efficient coverage and crystallinity of the CdS film on CdTe NRs arrays, which can reduce the recombination of electron–hole pairs at the interface. In this experiment, to further analyze the reason for the performance of different CdTe/CdS solar cells prepared using different methods, the shunt resistance (R_{sh}), sheet resistance (R_s), ideality factor (n), and reverse saturation current density (J_o) for the devices are also measured. It can be observed that the R_{sh} of all devices is not high, which will have significant restrictions on the V_{oc} of the as-synthesized solar cells. Therefore, the V_{oc} of all the devices is low. The limited J_{sc} of all devices may be attributed to several reasons such as poor CdTe/CdS interface, high contact resistance, and a large number of defects. Or, there are other problems that are unknown. Hence, in our future research, there is much work to do to improve the photovoltaic performance of the present devices.

Table 1. The performance parameters of CdTe thin film solar cells.

Samples	V_{oc}/V	J_{sc}/mA·cm^{-2}	FF	PCE/%	R_s/Ω	R_{sh}/Ω	n	J_o/mA·cm^{-2}
A CdTe/CBD-CdS	0.32	2.71	0.31	0.27	278.45	1101.54	1.12	2.94×10^{-5}
B CdTe/HP-CdS	0.37	7.00	0.34	0.88	323.86	2121.84	1.21	3.42×10^{-5}
C CdTe/MS-CdS	0.47	9.51	0.56	2.50	84.66	2387.25	1.23	2.19×10^{-6}

To further analyze the reason for the poor performance of different CdTe NRs/CdS solar cells prepared using different methods, the solar cell based on the CdTe thin film is fabricated, and the FESEM image and J–V curve of the CdTe thin film/CdS solar cell are shown in Fig. S2. As is seen, the CdS film exhibits excellent coverage on the top of the CdTe film, forming a better interface between the CdTe film and CdS in comparison with that of CdTe NRs and CdS. Therefore, it can be concluded that the interface of the CdTe and CdS has a great influence on the performance of the solar cell. It is well known that the $CdCl_2$ annealing process is one of the most widely adopted techniques owing to its advantageous effects which have been reported frequently in improving the quality of the interface and fabrication of high-efficiency CdTe/CdS photovoltaic devices.[29–31] The $CdCl_2$ is the active medium in the interdiffusion of the CdS-CdTe and promotes the formation of the CdS_xTe_{1-x} interfacial layer. This interfacial layer is generally believed to be beneficial to reduce the effects of lattice mismatch between the CdS and CdTe, which has major effects on the performance of devices.[32] Numerous studies show that annealing temperature plays a role in the formation of the CdS_xTe_{1-x} interfacial layer, which can affect the conversion efficiency of the device. Hence, to improve device performance, the as-synthesized CdTe/CdS composite films prepared by different methods are annealed at different temperatures.

FESEM images of the CdTe/CdS composite films annealed at different temperatures are shown in Figs. 6 and 7. When the CdTe/MS-CdS film is annealed at 350 °C (Fig. 5), the grain boundary of the CdS layer is obvious in comparison with the film annealed at 400 °C (Fig. 4), which can result in more recombination centers. The clear and sharp in-

terface between the CdS and CdTe also suggests an abrupt heterojunction.[33] When the temperature continues to increase, noteworthy changes can be observed. As can be seen in Fig. 7(a), when the CdTe/CBD-CdS films are annealed at 450 °C, the heterojunction of CdTe/CdS films is destroyed, voids become more distinctly visible at the interface of the CdTe and CdS layer, and the CdS layer is consumed. For the CdTe/HP-CdS films annealed at 450 °C, the degree of intermixing of the CdTe and CdS increases with increasing the annealing temperature, and it is difficult to identify the CdTe/CdS interface. A similar phenomenon can also be observed for CdTe/MS-CdS films, as depicted in Figs. 7(c) and 7(d). When the CdTe/MS-CdS films are annealed at 450 °C (Fig. 7(c)), CdTe NRs and CdS layer can be reluctantly distinguished, and when the temperature is further increased to 500 °C, the films also become indistinguishable and could no longer be identified as discussed earlier. Excessive interdiffusion can lead to deterioration in the device properties. In addition, in our experiment, when the temperature is above 500 °C, the CdTe/CdS composite films fail to adhere properly on the Ni substrate due to the linear coefficient of expansion gap between the Ni (12–14 $\times$ 10^{-6} °C) and CdTe (5.9 $\times$ 10^{-6} °C). On the basis of the above discussion, it can be concluded that the degree of interdiffusion at the interface of the CdS/CdTe depends on the film growth and annealing treatment. Particularly, when the films are annealed at high temperatures, the change of the CdS/CdTe interface has a lot to do with the growth of the CdS film. Consequently, to obtain a highly efficient solar cell, in-depth studies are still needed.

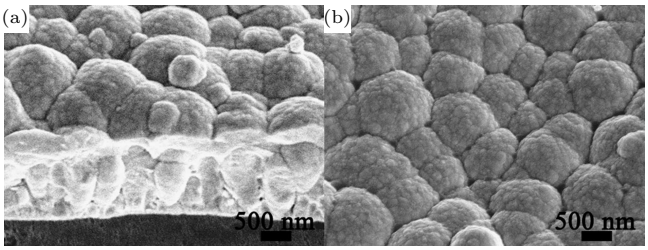

Fig. 6. The cross-section (a) and the top surface (b) FESEM images of CdTe/MS-CdS films annealed at 350 °C.

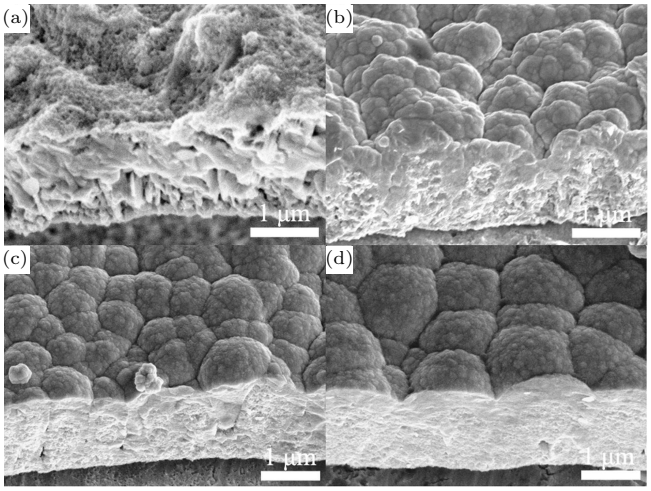

Fig. 7. FESEM images of CdTe/CdS films annealed at different temperatures: (a) CdTe/CBD-CdS films annealed at 450 °C, (b) CdTe/HP-CdS films annealed at 450 °C, (c) CdTe/MS-CdS films annealed at 450 °C, (d) CdTe/MS-CdS films annealed at 500 °C.

4. Conclusions

In summary, CdS films are successfully grown on CdTe NRs arrays by the CBD, HP, and MS methods. The growth of CdS films on CdTe NRs arrays is investigated in detail. Compared to the CBD and HP methods, an efficient coverage of CdS films with enhanced crystallization performance can be achieved by the MS method, forming a better contact between the CdS film and CdTe NRs. The performances of solar cells with different CdS layers are examined carefully. The best-performing device with a maximum efficiency of 2.50%, a J_{sc} of 9.51 mA/cm^2, V_{oc} of 0.47 V, and an FF of 0.56 is demonstrated. By carefully analyzing the photovoltaic parameters, the improvements in the efficiency can be ascribed not only to the better coverage and crystalline quality of the CdS film on CdTe NRs arrays, but also to a better interfacial property of CdS/CdTe. Besides, to further study the changes of the CdS/CdTe interface, the as-synthesized CdTe/CdS composite films prepared by different methods are annealed at different temperatures. After careful investigation, it can be found that the change of the CdS/CdTe interface has a lot to do with the CdS layer. In short, these results provide a bright future for material investigation, and improve the performance of solar cells.

References

[1] Akbarnejad T, Ghorannevis Z, Mohammadi E and Fekriaval L 2019 *J. Electroanal. Chem.* **849** 113358
[2] Ojo A A, Salim H I, Olusola O I, Madugu M L and Dharmadasa I M 2017 *J. Mater. Sci-Mater. El.* **28** 3254
[3] Stechmann G, Zaefferer S, Konijnenberg P, Raabe D, Gretener C, Kranz L, Perrenoud J, Buecheler S and Tiwari A N 2016 *Sol. Energ. Mat. Sol. C* **151** 66
[4] Sabet M, Niasari M S and Amiri O 2014 *Electrochim. Acta* **117** 504
[5] Vigil-Galán O, Pulgarín F A, Cruz-Gandarilla F, Courel M, Villarreal-Ruiz G, Sánchez Y, Jiménez-Olarte D and Saucedo E 2016 *Mater. Design* **99** 254
[6] Baghchesara M A, Yousefi R, Cheraghizade M, Jamali-Sheini F and Saáedi A 2016 *Ceram. Int.* **42** 1891
[7] Xie K, Wu Z, Wang M Y, Yu J D, Gong C, Sun L and Lin C J 2016 *Electrochem. Commun.* **63** 56
[8] Zhao G D, Sun M L, Liu X L, Xuan J Y, Kong W C, Zhang R N, Sun Y P, Jia F C, Yin G C and Liu B 2019 *Electrochim. Acta* **304** 334
[9] Wang J, Liu S R, Mu Y N, Liu L, A R N, Su P Y, Yang J D, Zhu G J, Fu W Y and Yang H B 2017 *J. Colloid. Interf. Sci.* **505** 59
[10] Li H and Liu X 2015 *Sol. Energy* **115** 603
[11] Senthamilselvi V, Saravanakumar K, Jabena Begum N, Anandhi R, Ravichandran A T, Sakthivel B and Ravichandran K 2012 *J. Mater. Sci-Mater. El.* **23** 302
[12] He X D, Wang Y, Jia K F and Zhang Y T 2016 *Mater. Lett.* **181** 244
[13] Peng W C, Li J, Chen B J, Wang N, Luo G H and Wei F 2016 *Catal. Commun.* **74** 39
[14] Yamamoto H, Aizawa M and Zhuang Z 2012 *Power Technol.* **222** 193
[15] Lin Z J, Zhu Q, Dong Y, Liu S H, Li J G, Li X D, Huo D, Zhang M, Xie M and Sun X D 2016 *Cryst. Eng. Comm.* **18** 3768

[16] Tao J H, Liu J F, Chen L L, Cao H Y, Meng X K, Zhang Y B, Zhang C J, Sun L, Yang P X and Chu J H 2016 *Green Chem.* **18** 550
[17] Guo Y X, Jiang J C, Zuo S H, Shi F W, Tao J H, Hu Z G, Hu X B, Hu G J, Yang P X and Chu J H 2018 *Sol. Energ. Mat. Sol. C* **178** 186
[18] Ravichandran K and Philominathan P 2009 *Appl. Surf. Sci.* **255** 5736
[19] Gao X F, Sun W T, Hu Z D, Zhang G A, Feng S, Li F and Peng L M 2009 *J. Phys. Chem. C* **113** 20481
[20] Esparza D, Zarazúa I, López-Luke T, Cerdán-Pasarán A, Sánchez-Solís A, Torres-Castro A, Mora-Sero I and Rosa E D 2015 *J. Phys. Chem. C* **119** 13394
[21] Mathew X, Enriquez J P, Romeo A and Tiwari A N 2004 *Sol. Energy* **77** 831
[22] Jaegermann W, Klein A, Fritsche J, Kraft D and Späth B 2005 *MRS Proceedings* **865** F6.1
[23] Morales-Acevedo A 2006 *Sol. Energy Mater. Sol. Cells* **90** 2213
[24] Enríquez J P, Barojas E G, González R S and Pal U 2007 *Sol. Energy Mater. Sol. Cells* **91** 1392
[25] Wang J, Liu S R and Mu Y N 2017 *J. Colloid. Interf. Sci.* **505** 1047
[26] Wang J, Liu S R and Meng X W 2017 *Electrochim. Acta* **258** 858
[27] Sun M, Fu W and Li Q 2014 *Rsc Adv.* **4** 7178
[28] Alexander J N, Higashiya S and Caskey D 2014 *Sol. Energy Mater. Sol. Cells* **125** 47
[29] Abbas A, Kaminski P, West G, Barth K, Sampath W S, Bowers J and Walls J M 2015 *MRS Proceedings* **1738** 7
[30] Abbas A, West G D, Bowers J W, Kaminski P M, Maniscalco B, Walls J M, Barth K L and Sampath W S 2014 *MRS Proceedings* **1638** 9
[31] Kumar S G and Rao K S R K 2014 *Energy Environ. Sci.* **7** 45
[32] Ferekides C S, Marinskiy D, Viswanathan V, Tetali B, Palekis V, Selvaraj P and Morel D L 2000 *Thin Solid Film* **361-362** 520
[33] Han J F, Fu G H and Krishnakumar V 2015 *Thin Solid Films* **582** 290